

Collisional excitation of methyl (iso)cyanide by He atoms: rate coefficients and isomerism effects

M. Ben Khalifa¹* P. J. Dagdigan² and J. Loreau¹†

¹*KU Leuven, Department of Chemistry, Celestijnenlaan 200F, B-3001 Leuven, Belgium.*

²*Department of Chemistry, The Johns Hopkins University, Baltimore, MD 21218-2685, USA.*

ABSTRACT

Among all closed-shell species observed in molecular clouds, molecules with C_{3v} symmetry play a crucial role, as their rotational spectroscopy allows them to behave as a gas thermometer. In the interstellar medium, methyl cyanide (CH_3CN) is the second most abundant of those (after ammonia, NH_3). Its isomer, methyl isocyanide (CH_3NC) is less abundant but has been detected in many astrophysical sources. In order to assess their absolute and relative abundances, it is essential to understand their collisional excitation properties. This paper reports the calculation of rate coefficients for rotational excitation of CH_3CN and CH_3NC molecules with He atoms, from low (5 K) to moderate (100 K) temperatures. We include the first 74 and 66 rotational states of both *para* and *ortho* symmetries of CH_3CN and CH_3NC , respectively. A propensity for $\Delta j = 2$ transitions is observed in the case of CH_3CN -He collisions, whereas in the case of CH_3NC -He a propensity for $\Delta j = 1$ is observed for transitions involving low values of j and at low temperatures, while a propensity for $\Delta j = 2$ is observed for higher values of j and at high temperatures. A comparison of rate coefficients shows differences up to a factor of 3, depending on temperature and on the *ortho/para* symmetries for dominant transitions. This confirms the importance of having specific collisional data for each isomer. We also examined the effect of these new rates on the CH_3CN and CH_3NC excitation in molecular clouds by performing radiative transfer calculations of the excitation and brightness temperatures for several detected lines.

Key words: radiative transfer - molecular data - abundance - ISM

1 INTRODUCTION

Among all molecules detected in astrophysical clouds, nitriles (or cyanides, $R-C\equiv N$) are the largest class of compounds. They represent about one-fifth of the more than 250 molecules identified to date in the interstellar medium (ISM) and circumstellar shells (Müller et al. 2001; McGuire 2022). Cyanides are readily detected in a number of interstellar environments thanks to their large dipole moments (Lee et al. 1972). Recently, even complex cyanides like hydroxyacetonitrile ($HOCH_2C\equiv N$) (Zeng et al. 2019) and the aromatic ring benzonitrile (C_6H_5CN) (McGuire et al. 2018) have been detected. In addition to nitrile molecules, a few isocyanides (with the functional group $-N\equiv C$) have also been detected in objects of the ISM. They include HNC (Bellili et al. 2019; Schilke et al. 2001), HNCO (Snyder & Buhl 1972), CH_3NC (Irvine & Schloerb 1984; Cernicharo et al. 1988; Remijan et al. 2005; Margulès et al. 2018; Calcutt et al. 2018) HCCNC (Kawaguchi et al. 1992), CH_2CHNC (tentatively) (López et al. 2014) as well as inorganic isocyanides Müller et al. (2001).

CH_3CN is one of the most ubiquitous interstellar organic molecules and one that is regularly detected. It was observed in a variety of low- and high-mass sources (Beltran et al. 2005; Zapata et al. 2010). CH_3CN was detected towards the massive star forming re-

gions Sagittarius A and B, close to the Galactic center (Pols et al. 2018). It has also been identified ubiquitously, e.g. in the TMC-1 dark cloud (Matthews & Sears 1983), the low-mass protostar IRAS 16293-2422 (Cazaux et al. 2003), in the circumstellar shell of the carbon-rich star IRC +10216 (Agúndez et al. 2008), and in comets such as Kohoutek (Ulich & Conklin 1974). Recently, large quantities of CH_3CN were detected in the protoplanetary disk surrounding the young star MWC-480 (Öberg et al. 2015). Thanks to its three-fold symmetry and its large dipole moment, CH_3CN is used as a gas thermometer to probe interstellar environments and it is a useful tracer of the dense gas (Wilner et al. 1994). Its isomer CH_3NC is thermodynamically the less stable isomer of CH_3CN by about 103 kJ/mol, with a barrier to isomerization of about 160 kJ/mol (Nguyen et al. 2018). CH_3NC was tentatively observed for the first time in the Sgr B2 cloud Cernicharo et al. (1988) and confirmed with additional transitions seventeen years later by Remijan et al. (2005). Since then, it has been observed only in a handful of sources, including the Horsehead nebula photodissociation region by Gratier et al. (2013) and Orion KL by López et al. (2014), among others (Margulès et al. 2018; Calcutt et al. 2018).

For typical dense cloud conditions, theoretical calculations of DeFrees et al. (1985) estimated the ratio of CH_3NC/CH_3CN to be in the range of 0.1-0.4. However, Cernicharo et al. (1988) deduced from their observations an abundance ratio of ~ 0.03 - 0.05 , showing that CH_3CN is an order of magnitude higher than previous estimates. Later, Gratier et al. (2013) found, according to their observations in

* E-mail: malek.benkhalifa@kuleuven.be

† E-mail: jerome.loreau@kuleuven.be

the Horsehead region, an abundance ratio $\text{CH}_3\text{NC}/\text{CH}_3\text{CN}$ in agreement with estimations of [DeFrees et al. \(1985\)](#).

In astrophysical media, the chemistry of CH_3CN is assumed to be governed by two processes: the dissociative recombination reaction $\text{CH}_3\text{CNH}^+ + e^- \rightarrow \text{CH}_3\text{CN} + \text{H}$, and by the radiative association mechanism $\text{CN} + \text{CH}_3 \rightarrow \text{CH}_3\text{CN} + h\nu$ ([McElroy et al. 2013](#); [Mackay 1999](#); [Willacy et al. 1993](#)), whereas gas-grain chemistry can also provide an important pathway for the formation of methyl cyanide, either from direct addition of CH_3 and CN or from successive hydrogenations starting with C_2N ([Belloche et al. 2009](#)). Acetonitrile and methyl isocyanide are isoelectronic symmetric top molecules which show close similarities in their molecular parameters such as the bond length ([Moffat 1964](#); [Costain 1958](#)) and electric dipole moment ([Lee et al. 1972](#)), which cannot introduce any bias in their respective rotational spectra. Therefore, the formation and evolution of interstellar clouds and the stars they generate can be explored through isomer comparison studies.

In order to identify molecules in the ISM and their densities, a precise determination of the positions and intensity of spectral lines is necessary. Although the vibration-rotation spectrum of both CH_3CN and CH_3NC is well established, their collisional properties are not well constrained, which can lead to errors on the inferred densities.

In the ISM, the local thermodynamic equilibrium (LTE) conditions are usually not fulfilled ([Roueff & Lique 2013](#)). Therefore, both collisional and radiative processes should be considered in the molecular line modeling in order to derive relative abundances or column densities of $\text{CH}_3\text{CN}/\text{NC}$ as well as the physical conditions of the gas. Einstein coefficients corresponding to radiative processes are usually available in literature; however, collisional rates between $\text{CH}_3\text{CN}/\text{NC}$ with the most abundant species (H_2 , H and He) have to be computed.

To the best of our knowledge, the only rate coefficients for $\text{CH}_3\text{CN-He}/\text{H}_2$ that are available in literature have been computed by [Green \(1986\)](#). These collisional rate coefficients are based on the Infinite Order Sudden (IOS) approximation, without any potential calculation, which can lead to large errors. In addition, the rates published by Green begin at a temperature of 20 K, preventing a precise modelling in the dense molecular clouds, with a typical temperature around 5 K. Moreover, concerning the isomer CH_3NC , no collision rate coefficients seem to be available and the interpretation of astrophysical observation is always realized by using rate coefficients of CH_3CN .

For a precise determination of the absolute and relative abundance of methyl (iso)cyanide, we present in this paper the first rate coefficients for the collision excitation of CH_3NC , which we compare to those obtained for CH_3CN to highlight isomerism effects. We restrict ourselves to the collisional excitation of the rigid symmetric top molecules CH_3CN and its isomer CH_3NC with He atoms, which are investigated with the same computational method.

The overall structure of this paper is as follows: first, we present in section 2, a brief description of the *ab initio* calculations of $\text{CH}_3\text{CN}/\text{NC-He}$ systems used in this work. Section 3 describes the scattering calculations. We illustrate inelastic collisional rate coefficients of $\text{CH}_3\text{CN-He}$ and $\text{CH}_3\text{NC-He}$ complexes in section 3.2. We analyze the effect of our rate coefficients by performing a radiative transfer calculation for typical interstellar conditions in section 4. Conclusions and future outlooks are drawn in Section 5.

2 POTENTIAL ENERGY SURFACES

Recently, 3-dimensional potential energy surfaces (PESs) were obtained by [Ben Khalifa et al. \(2022\)](#), for the symmetric top molecules

CH_3CN and CH_3NC in their ground electronic state (\bar{X}^1A_1) interacting with He atoms. The PESs were computed using the explicitly correlated coupled cluster CCSD(T)-F12a method ([Knizia et al. 2009](#)) in conjunction with the aug-cc-pVTZ basis set ([Dunning Jr 1989](#)) as implemented in the MOLPRO package ([Werner et al. 2015](#)). The CH_3CN and CH_3NC molecules were considered as rigid rotors with the internal coordinates of methyl (iso)cyanide frozen at their experimental equilibrium values for the vibrational ground state.

To compute the interaction potentials, we chose the center of mass (c.m.) of CH_3CN and CH_3NC molecules to be the origin of the coordinate system, and we have characterized the orientations of each complex by R , θ and ϕ , where R represents the distance between the center of mass of $\text{CH}_3\text{CN}/\text{NC}$ and the He atom, θ is the angle between \mathbf{R} and the C_3 axis of the molecule, and ϕ is the azimuthal angle that describes the rotation of the He atom around the C_{3v} axis.

The global minimum for the $\text{CH}_3\text{CN-He}$ PES is located at the configuration $\phi = 60^\circ$, $\theta = 100^\circ$ and $R = 6.15$ bohr with a well depth of 55.10 cm^{-1} , while the global minimum of the $\text{CH}_3\text{NC-He}$ PES has a well depth of 58.61 cm^{-1} located at $\phi = 60^\circ$, $\theta = 100^\circ$ and $R = 6.05$ bohr. These features are similar to those of PESs for other symmetric top + rare gas atom systems such as NH_3 with He , Ne , Ar , Kr , Xe and $\text{SiH}_3\text{CN-He}$ ([Loreau et al. 2014](#); [Loreau & van der Avoird 2015](#); [Naouai et al. 2021](#)). The potential energy surfaces of $\text{CH}_3\text{CN-He}$ and $\text{CH}_3\text{NC-He}$ were fitted using the procedure given by [Green \(1976\)](#) for the $\text{NH}_3\text{-He}$ system. The dependence of the PESs on the $\text{He-CH}_3\text{CN}$ and $\text{He-CH}_3\text{NC}$ angles was fitted by the usual spherical harmonic expansion (see Eq 1). From an *ab initio* grid containing 19 θ -values and 7 ϕ -values, we end up with 70 terms with $l_{max}=18$, with a deviation between *ab initio* potentials and analytical form less than 1%.

$$V(R, \theta, \phi) = \sum_{l=0}^{l_{max}} \sum_{m=0}^l V_{lm}(R) \frac{Y_l^m(\theta, \phi) + (-1)^m Y_l^{-m}(\theta, \phi)}{1 + \delta_{m,0}} \quad (1)$$

The shape and magnitude of the radial coefficients V_{lm} reflect the stronger anisotropy of the interaction potential of $\text{CH}_3\text{NC-He}$ compared to $\text{CH}_3\text{CN-He}$. While the global minimum of the PES is deeper for $\text{CH}_3\text{NC-He}$ than for $\text{CH}_3\text{CN-He}$, the isotropic term is less deep for $\text{CH}_3\text{NC-He}$ (56.2 cm^{-1}) than $\text{CH}_3\text{CN-He}$ (65.8 cm^{-1}). Furthermore, for odd values of l , the radial coefficients are larger for $\text{CH}_3\text{NC-He}$ than for $\text{CH}_3\text{CN-He}$, however, V_{lm} with even values of l are larger for CH_3CN than those for CH_3NC in the medium and long-range of distances R , and smaller at short range. This is expected to have an effect on the propensity rules in the rotational excitation, as shall be further discussed in section 3.2.

All technical details concerning the *ab initio* PESs, potential well depths and their accurate locations as well as the fitting procedure, can be found in [Ben Khalifa et al. \(2022\)](#) (hereafter Paper I).

3 SCATTERING CALCULATIONS

3.1 Cross sections

Scattering calculations corresponding to rotational (de-)excitation of CH_3CN and CH_3NC molecules by collision with He atoms were performed for kinetic energies ranging from 0.1 to 900 cm^{-1} .

Methyl (iso)cyanide is a prolate symmetric top molecule. The rotational levels structure associated to both isomers were obtained using the B and A rotational constants fit on experimental spectra, which are equal to 0.3353 and 5.2420 cm^{-1} for CH_3NC [Margulès et al. \(2001\)](#) and 0.3068 and 5.2470 cm^{-1} for CH_3CN

(Remijan & Markwick-Kemper 2007) and are function of two quantum numbers, j and k , where j is the rotational angular momentum and k is a pseudo quantum number associated to the projection of j on the body-fixed z axis. Due to the centrifugal distortion, the rotational energy deviation between two adjacent j -levels decreases when k increases. Therefore, it is possible to find multiple lines with various excitation energies in one spectrum, which makes CH_3CN a good probe of the local temperature. The state of the nuclear spin associated to hydrogen atoms determines whether CH_3CN and CH_3NC have *para* (E) or *ortho* (A) symmetry. The spectral signatures are linked to k -ladder structures whose notation for the *ortho* configuration is $k=3n$ and for the *para* configuration is $k=3n \pm 1$, n being an integer. As the *ortho* and *para* levels of CH_3CN and CH_3NC cannot interchange in inelastic collisions, the state-to-state cross sections were computed separately for each nuclear spin species.

The most accurate method to compute state-to-state cross sections is the close-coupling (CC) approach. However, due to the small spacing between rotational levels and the fact that transitions involving highly excited rotational states have been observed (up to $j = 18$), a large rotational basis set of CH_3CN and CH_3NC is needed, which makes the use of the full CC method (Arthurs & Dalgarno 1960) extremely expensive in computational time with increasing energy. In order to achieve a good compromise between the accuracy of the results and computational cost, the collisional cross sections were calculated using the CC method for $E_{\text{tot}} \leq 100 \text{ cm}^{-1}$, and with the coupled-state (CS) approximation (McGuire & Kouri 1974) for higher energies, up to $E_{\text{tot}}=900 \text{ cm}^{-1}$ using both MOLSCAT (Hutson & Le Sueur 2019) and HIBRIDON (Alexander et al. 2023) codes. We carried out convergence tests at different energies in order to guarantee the validity of CS approximation, as presented in Table 1. As reported, the relative error between CC and CS approximation for several transitions does not exceed 10% for $E_{\text{tot}}= 100 \text{ cm}^{-1}$ and 5% for $E_{\text{tot}}= 300 \text{ cm}^{-1}$. Furthermore, CPU time and disk occupancy for CS computations are almost five times smaller than CC ones. Globally, the CS approximation reduced the computational cost without a significant loss of accuracy, especially at high collision energy.

For astrophysical purposes, the highest rotational levels to be converged in our scattering calculations are $j_k=16_6$ for *ortho*- $\text{CH}_3\text{NC}/\text{CN}$ (with $E_{\text{rot}}= 267.84 \text{ cm}^{-1}$ and 262.07 cm^{-1} , respectively) and $j_k=16_5$ for *para*- $\text{CH}_3\text{NC}/\text{CN}$ (with $E_{\text{rot}}= 213.87 \text{ cm}^{-1}$ and 207.52 cm^{-1}), respectively. To do so, the rotational basis set has been extended enough to ensure the convergence of the collisional cross-sections.

The number of rotational levels N considered for our computations was taken as : $N = 35$ (up to $j_k=20_0$ with an energy of 140.8 cm^{-1}) for total energies $E_{\text{tot}} \leq 50 \text{ cm}^{-1}$, $N = 55$ (up to $j_k=26_0$ with an energy of 235.4 cm^{-1}) for total energies $50 \text{ cm}^{-1} \leq E_{\text{tot}} \leq 100 \text{ cm}^{-1}$, and $N = 120$ (up to $j_k=29_9$ with an energy of 689.17 cm^{-1}) for $100 \text{ cm}^{-1} \leq E_{\text{tot}} \leq 300 \text{ cm}^{-1}$ for *ortho*- CH_3NC , while for *ortho*- CH_3CN it was necessary to select $N = 55$ (all levels up to $j_k= 12_6$, energy of 225.6 cm^{-1}) for total energies $E_{\text{tot}} \leq 50 \text{ cm}^{-1}$, 65 (up to $j_k= 29_3$ energy of 311.4 cm^{-1}) for $50 \text{ cm}^{-1} \leq E_{\text{tot}} \leq 100 \text{ cm}^{-1}$, and 115 (up to $j_k=35_6$ with an energy of 564.33 cm^{-1}) for $100 \text{ cm}^{-1} \leq E_{\text{tot}} \leq 300 \text{ cm}^{-1}$. At the largest total energy considered (900 cm^{-1}), the rotational basis were extended to $N = 160$ or $N = 150$, for CH_3NC and CH_3CN , respectively.

For *para*- $\text{CH}_3\text{NC-He}$, we take $N = 65$ (up to $j_k= 13_5$, with an energy of 183.7 cm^{-1}) for $E_{\text{tot}} \leq 50 \text{ cm}^{-1}$, $N = 75$ (up to $j_k= 20_4$ with an energy of 219.3 cm^{-1}) for $50 \text{ cm}^{-1} \leq E_{\text{tot}} \leq 100 \text{ cm}^{-1}$, $N = 145$ (up to $j_k= 17_8$ with an energy of 416.63 cm^{-1}) for $100 \leq E_{\text{tot}} \leq 300$ and $N = 180$ (up to $j_k = 14_{10}$ with an energy of

Table 1. Comparison between CC and CS cross sections (in \AA^2) for the excitation of *para* and *ortho* CH_3NC by He for total energies $E_{\text{tot}}=100$ and 300 cm^{-1} (For $E_{\text{tot}}=300 \text{ cm}^{-1}$, total angular momenta J up to 20 are considered).

Molecule	Energy	$j_k \rightarrow j'_k$	CC	CS
o- CH_3NC	$E=100 \text{ cm}^{-1}$	$0_0 \rightarrow 1_0$	7.208	7.042
		$0_0 \rightarrow 2_0$	14.36	14.11
		$0_0 \rightarrow 3_0$	2.742	2.944
		$0_0 \rightarrow 4_0$	8.407	8.016
o- CH_3NC	$E=300 \text{ cm}^{-1}$	$0_0 \rightarrow 1_0$	0.500	0.498
		$0_0 \rightarrow 2_0$	1.089	0.981
		$0_0 \rightarrow 3_0$	0.307	0.290
		$0_0 \rightarrow 4_0$	0.983	0.950
p- CH_3NC	$E=100 \text{ cm}^{-1}$	$1_1 \rightarrow 2_1$	8.342	8.628
		$1_1 \rightarrow 3_1$	9.847	10.13
		$1_1 \rightarrow 4_1$	2.887	3.091
		$1_1 \rightarrow 5_1$	7.887	7.438
p- CH_3NC	$E=300 \text{ cm}^{-1}$	$1_1 \rightarrow 2_1$	0.475	0.465
		$1_1 \rightarrow 3_1$	0.535	0.526
		$1_1 \rightarrow 4_1$	0.585	0.571
		$1_1 \rightarrow 5_1$	0.527	0.420

561.085 cm^{-1}) for $300 \leq E_{\text{tot}} \leq 900 \text{ cm}^{-1}$, while for *para*- CH_3CN , we take $N = 78$ for $E_{\text{tot}} \leq 100 \text{ cm}^{-1}$ (up to $j_k= 18_7$, with an energy 346.9 cm^{-1}) and $N = 202$ for $100 \text{ cm}^{-1} \leq E_{\text{tot}} \leq 900 \text{ cm}^{-1}$ (up to $j_k= 14_{13}$, with an energy 898.8 cm^{-1}). The maximum value of the total angular momentum J was selected such that the inelastic cross sections are all converged to within 0.05 \AA^2 . Finally, the integral cross sections were obtained by summing all partial cross sections over the total angular momentum J until reaching the convergence.

We computed collisional cross sections for total energy ranging from 0.1 to 900 cm^{-1} . In order to describe the resonances in the cross sections, we used a smaller energy step dE at low collision energy and a larger energy step as the collisional energy increases and the resonances vanish. We used an energy step dE of 0.2 cm^{-1} for energies below 50 cm^{-1} , 0.5 cm^{-1} for energies between 50 cm^{-1} and 100 cm^{-1} , 2 cm^{-1} for energies between 100 cm^{-1} and 200 cm^{-1} , 5 cm^{-1} for energies between 200 cm^{-1} and 400 cm^{-1} , and 10 cm^{-1} for energies between 400 cm^{-1} and 900 cm^{-1} .

3.2 Rate coefficients

From the collisional cross-sections $\sigma_{i \rightarrow f}(E_c)$, we derive the corresponding collisional rate coefficients k_{if} at a temperature T by an average over a Maxwellian distribution of kinetic energy as expressed:

$$k_{i \rightarrow f}(T) = \left(\frac{8}{\pi \mu \beta} \right)^{\frac{1}{2}} \beta^2 \int_0^{\infty} E_c \sigma_{i \rightarrow f}(E_c) e^{-\beta E_c} dE_c \quad (2)$$

Where $\beta=1/k_B T$, and k_B , T and $\mu = 3.646815237 \text{ a.u}$ denote the Boltzmann constant, the kinetic temperature and the reduced mass of the system, respectively.

For $\text{CH}_3\text{CN-He}$ and $\text{CH}_3\text{NC-He}$, the state-to-state cross sections computed for total energy up to 900 cm^{-1} leads to converged collisional rate coefficients for the first 74 *para* levels and 66 *ortho* levels of each isomer up to a kinetic temperature $T = 100 \text{ K}$. This complete set of (de-)excitation rate coefficients will be made available online on the LAMDA, BASECOL and EMAA websites.

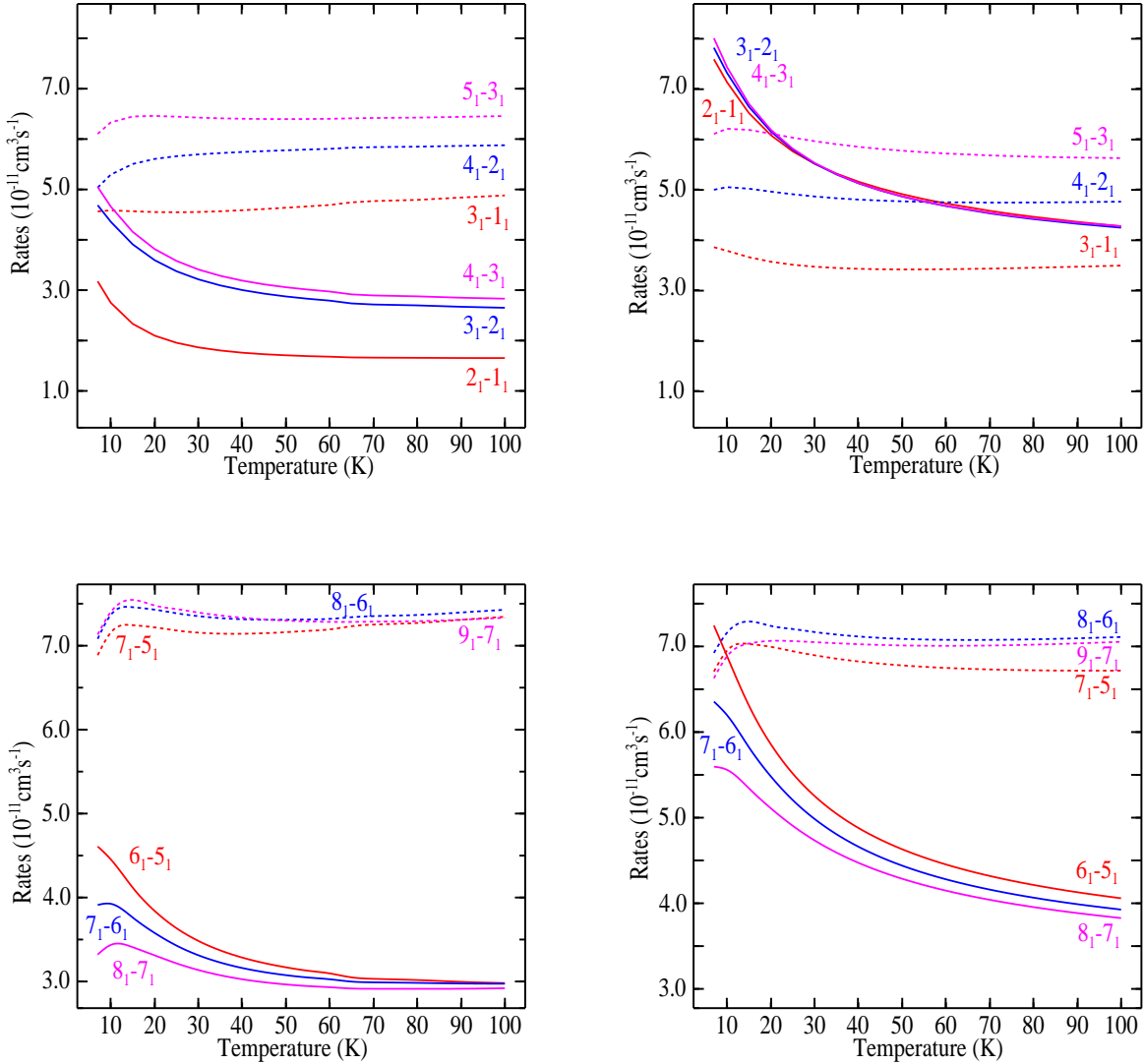


Figure 1. Temperature dependence of the rotational de-excitation rate coefficients for transitions $j_k \rightarrow j'_k$, of *para*-CH₃CN-He (left panels) and *para*-CH₃NC-He (right panels) induced by collisions with He. Top panels: comparison of $\Delta j = 1$ and $\Delta j = 2$ transitions with $j' = 1 - 3$ and $k = k' = 1$; Bottom panels: Same but with $j' = 5 - 7$.

We present in Fig. 1, the temperature variation of CH₃CN-He and CH₃NC-He state-to-state rate coefficients as a function of the temperature for selected transitions. We focus specifically on dipolar ($\Delta j=1$) and quadrupolar ($\Delta j=2$) transitions with $k = k' = 1$ in *para*-CH₃CN/NC. One can observe that there are significant differences between the CH₃CN-He and CH₃NC-He rate coefficients and that the propensity rules observed in the two sets of collisional rates are different.

The rate coefficients for CH₃CN-He associated to $\Delta j = 1$ transitions are considerably smaller than those for CH₃NC-He transitions, while those for $\Delta j = 2$ are of similar magnitude. This difference can be understood on the basis of the expansion terms in Eq. 1, and in particular the fact that the term V_{10} that drives $\Delta j = 1$ transitions is much larger for CH₃NC-He than for CH₃CN-He, as already discussed in Paper I. Overall the PES of CH₃NC-He is deeper but it also has a larger degree of anisotropy than the PES of CH₃CN-He,

leading to larger rate coefficients for $\Delta j = 1$ transitions. For CH₃CN-He, the $\Delta j = 2$ transitions dominate over $\Delta j = 1$ transitions at all temperatures.

On the other hand, for CH₃NC-He the dominant transitions are those associated with $\Delta j = 1$ at low temperature, and $\Delta j = 2$ at higher temperatures, leading to propensity rules that depend on the temperature. In addition, when the value of j increases, the transitions $\Delta j = 2$ become more and more dominant, including at low temperature. We can interpret this again based on the expansion of the PES. As discussed in Paper I, the V_{10} term is the dominant term for CH₃NC-He at low energies (up to about 40 cm^{-1}), while V_{20} dominates at higher energies. As a result, for highly excited rotational levels V_{20} it always the dominant term in the expansion and $\Delta j = 2$ transitions are favored.

While Fig. 1 only illustrates rate coefficients for *para*-CH₃CN/NC-He and for transitions with $k = k' = 1$, the same

behavior is also observed for other values of k as well as for *ortho*-CH₃CN/NC-He.

Because of the absence of rate coefficients for the excitation of CH₃NC, the collisional data for CH₃CN are often used in radiative transfer models to estimate the abundance of CH₃NC in the interstellar medium. In order to examine the validity of such an approach and the impact of isomerism effects in the collisional studies, we present in Fig 2 a systematic comparison of CH₃CN-He and CH₃NC-He rate coefficients, computed using the same level of theory (from *ab initio* to dynamics calculations). The comparison includes collisional rate coefficients for transitions among the first 50 *ortho* levels and 63 *para* levels of CH₃CN and CH₃NC at two temperatures, $T = 20$ K and $T = 100$ K.

The rate coefficients for the dominant transitions ($k > 10^{-11}$ cm³) of the two isomers are within a factor of 2, but significant differences exist for the smaller rate coefficients with relative deviations that can reach a factor of more than 3. Given the propensity rules discussed above, it is interesting to compare the excitation of CH₃CN and CH₃NC in more detail. Figure 2 reveals that the dominant transitions all correspond to $\Delta k = 0$ transitions. This can be explained by the fact that for symmetric tops these transitions are driven by the terms with $m = 0$ in the expansion (1), which are the largest ones, while transitions with $\Delta k = 1$ require terms with $m = 3$, which are small (Loreau & van der Avoird 2015; Ben Khalifa et al. 2022). The plots in Fig. 2 also show the clear propensity for $\Delta j = 2$ transitions in the case of CH₃CN-He, while for CH₃NC-He the rate coefficients for $\Delta j = 1$ and $\Delta j = 2$ are of similar magnitude. This reflects the fact that for CH₃NC-He, for low j the $\Delta j = 1$ transitions dominate, while the reverse is true for high values of j . Furthermore, the rates coefficients for $\Delta j = 2$, $\Delta k = 0$ transitions are larger for CH₃CN-He than for CH₃NC-He while the reverse is true for $\Delta j = 1$, $\Delta k = 0$ as well as $\Delta j = 4$, $\Delta k = 0$ and $\Delta j = 6$, $\Delta k = 0$. The transitions corresponding to $\Delta j = 3$, $\Delta k = 0$ and $\Delta j = 5$, $\Delta k = 0$ are similar in the case of *ortho*-CH₃CN/NC-He but larger for *para*-CH₃CN-He than *para*-CH₃NC-He.

The present results confirms that collisional rates should be obtained independently for different isomers and confirms previous results on isomerism effects found for other cyanides and isocyanides, such as HCN/HNC (Dumouchel et al. 2010), HC₃N/HC₂NC/HNC₃ (Bop et al. 2019) AICN/AINC and MgCN/MgNC (Hernández Vera et al. 2013). The rate coefficients obtained for the CH₃CN and CH₃NC isomers allow us to predict that the excitation of these species in the interstellar medium is different and that the abundance ratio of these molecules cannot be obtained by examining only the brightness temperature ratio of the lines. Therefore, a radiative transfer study must be performed for both isomers using their respective set of collisional rates coefficients to obtain the relative abundance of the two isomers with a good precision.

3.3 Comparison with previous results

Due to the importance of the CH₃CN molecule, and its omnipresence, a set of rate coefficients for the collisional de-excitation by H₂ molecules has been calculated by Green (1986), although using a very approximate treatment of both the *ab initio* potential and of the nuclear dynamics. To the best of our knowledge, these are the only rate coefficients known for this system and used in non-LTE radiative transfer modelling. It is therefore instructive to compare our results to those of Green (1986).

Because of the spherical character of *para*-H₂ ($j = 0$), we compare collisional rates of CH₃CN-H₂ with those with helium atoms,

duly scaled by a factor ~ 1.39 that reflects the difference in reduced masses. Figure 3 highlights the quenching rates computed at temperatures of 20 K and 100 K among the lowest 50 levels of *ortho*-CH₃CN-He and the lowest 50 levels of *para*-CH₃CN-He. We note that the collisional rate coefficients differ greatly, with differences that can reach three orders of magnitude for numerous transitions. The discrepancy is seen to be larger at low temperature (20 K) than at high temperature (100 K).

Globally, rate coefficients computed by Green are lower than the present results. Two main reasons can explain such large differences: (i) the use of two different interaction potentials, the potential of Green having been obtained with an approximate electron gas method; and (ii) the treatment of the dynamics. The present work uses either an accurate quantum approach (CC) or an approximate quantum approach (CS) whose validity has been tested for the present system. The rate coefficients computed by Green were obtained within the infinite order sudden (IOS) approximation for only 12 collision energies, which does not appear to be accurate in the case of CH₃CN-He. The difference in accuracy between the CS and IOS methods is expected to decrease with increasing energy, which likely explains the slightly better agreement at 100 K compared to 20 K. The large difference between collisional rates computed by Green compared to our CH₃CN-He rates calls for a re-examination of their impact on the abundance of CH₃CN in various astrophysical environments.

4 ASTROPHYSICAL APPLICATION

The comparison of collisional rate coefficients performed in section 3.2 showed that CH₃CN and its isomer CH₃NC have different excitation behaviors when they collide with helium atoms. It is therefore instructive to study the impact of using the appropriate rate coefficients when deriving the abundance of CH₃CN and CH₃NC in astrophysical environments.

As a first application, we performed a radiative transfer computation to simulate the excitation of both isomers within the escape probability formalism approximation for a uniform spherical geometry of a homogeneous interstellar medium as implemented in the RADEX code (Van der Tak et al. 2007). The molecular data (for CH₃CN and CH₃NC) are composed of rate coefficients (from 5 to 100K) scaled from He to H₂ and supplemented by the energy levels, Einstein coefficients, as well as line frequencies of both isomers. These spectroscopic data were obtained from the Cologne Database for Molecular Spectroscopy (CDMS) portal (Endres et al. 2016). We first computed the critical density of colliders $n^*(H_2, T)$ using the equation:

$$n^*(H_2, T) = \frac{A_{fi}}{\sum_{f \neq i} k_{fi}} \quad (3)$$

where k_{fi} and A_{fi} are collisional rate coefficients and Einstein spontaneous absorption coefficients, respectively.

The critical density was computed for transitions involving the emission in the range of 91.98 GHz and 220.74 GHz for CH₃CN and 100.52 GHz and 241.23 GHz for CH₃NC, covering lines that are often detected with ground based radio telescopes. This range of frequency includes the often detected transitions $j_k = 5 \rightarrow 4$ and $12 \rightarrow 11$ with k or $k' = 0, 1, 2$ and 3. The critical densities of colliders (in cm⁻³), computed at $T = 10, 50$ and 80K, are given in table 2. It is noticeable that the critical density of these observed transitions is around $\sim 10^4$ cm⁻³, which corresponds to the typical density of the interstellar medium. Therefore, the local thermodynamic equilibrium

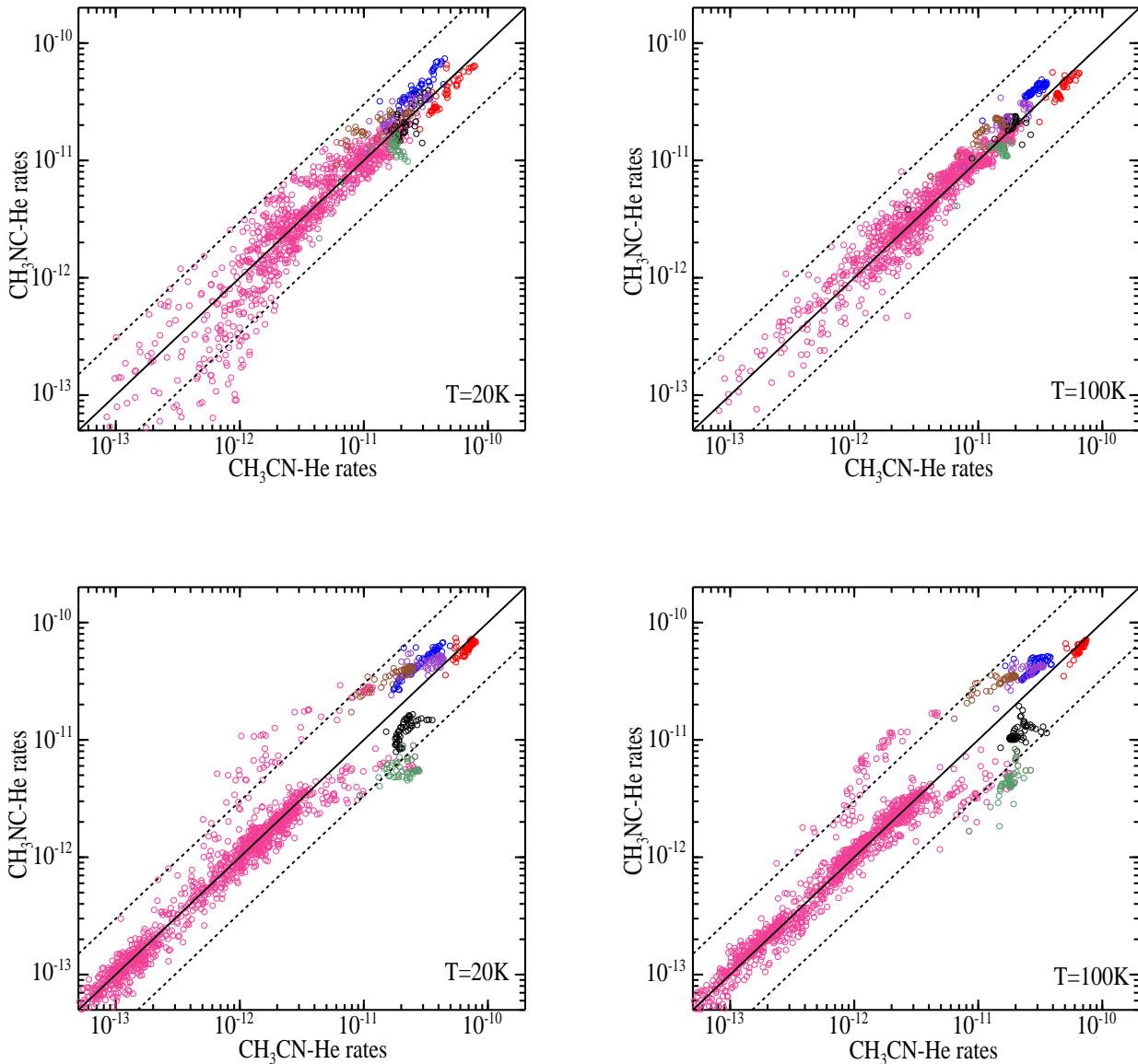


Figure 2. Comparison between *ortho* (top panels) and *para* (bottom panels) $\text{CH}_3\text{CN-He}$ and $\text{CH}_3\text{NC-He}$ rate coefficients at $T = 20 \text{ K}$ and $T = 100 \text{ K}$. The diagonal line corresponds to equal rate coefficients. Blue circles: transitions $\Delta j = 1, \Delta k = 0$; Red circles: $\Delta j=2, \Delta k=0$; Black circles: $\Delta j=3, \Delta k=0$; Purple circles: $\Delta j=4, \Delta k=0$; Green circles: $\Delta j=5, \Delta k=0$; Brown circles: $\Delta j=6, \Delta k=0$; Pink circles : all remaining quenching transitions ($\Delta j=1,2,3,\dots, \Delta k=1,2,3,\dots$)

cannot be assumed to be reached. Consequently, the use of non-LTE simulations is important in order to accurately model the CH_3CN and CH_3NC emission spectra.

We calculated the brightness temperature (T_B) and the excitation temperature (T_{ex}) for various pure rotational emission lines which are frequently observed in astrophysical clouds. We take here as examples the $j_k=2 \rightarrow 1, 5 \rightarrow 4$ and $6 \rightarrow 5$ with $k = 0, 1, 2$ and 3 transitions.

In the radiative transfer computation, the cosmic microwave background was introduced as a background radiation field ($T_{\text{CMB}}=2.73 \text{ K}$). The line width at the half-maximum (FWHM) was fixed at 25.0, 6.0 and 9.2 km.s^{-1} for $j_k=2 \rightarrow 1, 5 \rightarrow 4$ and $6 \rightarrow 5$ respectively

(Blackman et al. 1977; Araya et al. 2005), and the kinetic temperature was set at 20, 50 and 80 K.

In order to cover the H_2 volume density [$n(\text{H}_2)$] and to check the behavior of CH_3CN and CH_3NC excitation under and out of LTE conditions, we varied $n(\text{H}_2)$ from 10^2 cm^{-3} to 10^8 cm^{-3} and the column densities of CH_3CN and CH_3NC were fixed at $N_c=10^{14} \text{ cm}^{-2}$, a choice that is based on the molecule's estimated column density of both isomers in the ISM (Araya et al. 2005). However, a variation up to an order of magnitude of this quantity does not affect the magnitude of the excitation temperatures because of the optically thin regime.

Figure 4 presents the logarithm of the excitation temperature obtained for the transition $j_k = 2_1 \rightarrow 1_1$ using rate coefficients of *para*

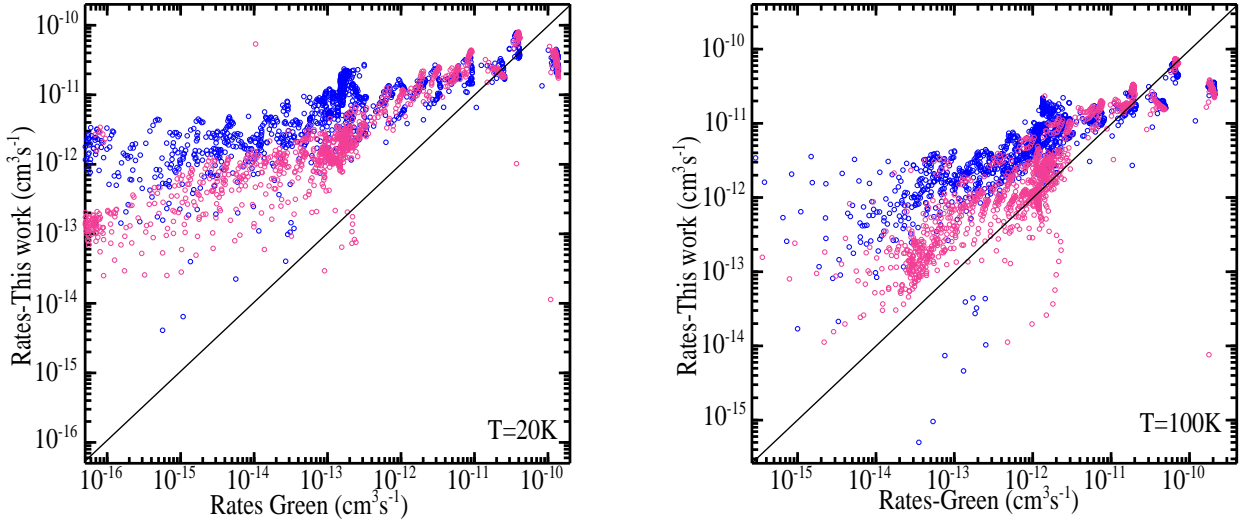


Figure 3. Comparison of quenching rate coefficients obtained in the present work and the published LAMDA rates from Green (1986) for transitions among the lowest 50 levels of *ortho*-CH₃CN-He (blue circles) and *para*-CH₃CN-He (pink circles) at $T = 20$ K and $T = 100$ K.

CH₃CN/NC computed during this work and CH₃CN rates computed by Green at $T = 20$ K. As can be seen in the figure, a population inversion is present for both isomers, which depends on the H₂ density, when we use the new set of collisional rates. One can see that the excitation temperature is negative in the H₂ density range of 10^4 - 10^6 cm⁻³. This negative excitation temperature behavior indicates a population inversion ($n_u/g_u > n_l/g_l$). However, this behavior is not predicted using the rate coefficients from the literature. The excitation temperature increases smoothly and tends towards the kinetic temperature, and no population inversion is observed when we use rates of Green. Consequently, a reexamination of the temperatures assigned to low density gases might be required.

Figure 5 displays the excitation temperature obtained for the transitions $j_k = 5 \rightarrow 4$ with $k = 0, 1, 2$ and 3. At low H₂ density, the medium is dilute and the excitation temperature is equal to $T_{\text{CMB}} = 2.73$ K, a value that corresponds to the background radiation field. It increases monotonically as collisional processes become more important predicting no suprathermal excitation at $T = 20$ K. For densities above $n_{\text{H}_2} = 10^6$ cm⁻³, the excitation temperature tends towards the kinetic temperature as LTE conditions are reached. At this stage, the populations of the rotational levels no longer depend on the density of H₂ and simply obey Boltzmann's law. Furthermore, at $T = 50$ K and 80 K, we note a particular suprathermal excitation for all transitions for H₂ densities between 10^5 and 10^6 cm⁻³. This behavior is defined by an excitation temperature (T_{ex}) that is greater than the kinetic temperature (T_k). For the transition $j_k = 5_3 \rightarrow 4_3$ of CH₃NC we observe a level population inversion where the excitation temperature becomes negative in approximately the same H₂ density range.

If we analyze the intermediate domain where collisional and radiative processes are in competition, we see that the comparison of the T_{ex} of CH₃CN and CH₃NC isomers shows that the excitation conditions of both isomers are different and that a similar T_{ex} for both isomers cannot be assumed.

Figure 6 presents the brightness temperature of CH₃CN and its isomer CH₃NC as a function of the H₂ volume density. In all panels, the brightness temperature globally increases with the increase of

Table 2. CH₃CN and CH₃NC critical densities n_c^* (cm⁻³) at 10, 50 and 80 K for several observed transitions.

Molecule	Transition	$T = 10$ K	$T = 50$ K	$T = 80$ K
CH ₃ CN	$5_0 \rightarrow 4_0$	0.3768×10^4	0.3976×10^4	0.4021×10^4
	$5_1 \rightarrow 4_1$	0.3732×10^4	0.3940×10^4	0.4001×10^4
	$5_2 \rightarrow 4_2$	0.3731×10^4	0.3939×10^4	0.4001×10^4
	$12_0 \rightarrow 11_0$	0.5568×10^5	0.5889×10^5	0.6097×10^5
	$12_1 \rightarrow 11_1$	0.6284×10^5	0.6487×10^5	0.6592×10^5
	$12_2 \rightarrow 11_2$	0.6283×10^5	0.6485×10^5	0.6590×10^5
CH ₃ NC	$5_0 \rightarrow 4_0$	0.4984×10^4	0.5037×10^4	0.5118×10^4
	$5_1 \rightarrow 4_1$	0.5492×10^4	0.5547×10^4	0.5684×10^4
	$5_2 \rightarrow 4_2$	0.4802×10^4	0.4924×10^4	0.5046×10^4
	$12_0 \rightarrow 11_0$	0.7128×10^5	0.7151×10^5	0.7266×10^5
	$12_1 \rightarrow 11_1$	0.8478×10^5	0.8520×10^5	0.8610×10^5
	$12_2 \rightarrow 11_2$	0.8333×10^5	0.2487×10^5	0.8543×10^5

the density and the temperature with an asymptotic behavior at $n > 10^6$ cm⁻³. A small peak is observed for $T = 50$ K and $5 \times 10^4 \leq n_{\text{H}_2} \leq 5 \times 10^5$ cm⁻³ with a higher magnitude at $T = 80$ K. We can see several differences between the two isomers, especially in the intermediary domain ($10^4 \leq n \leq 10^6$ cm⁻³) where collisional and radiative processes are in competition. These differences demonstrate the need of calculating collision rate coefficients of each isomer separately to determine their abundance with good precision.

5 CONCLUSION

State-to-state cross sections for the (de-)excitation of CH₃CN and its isomer CH₃NC induced by collisions with helium atoms were computed using the CC method for $E_{\text{tot}} \leq 100$ cm⁻¹ and CS approximation for $100 \leq E_{\text{tot}} \leq 900$ cm⁻¹. The dynamics was studied

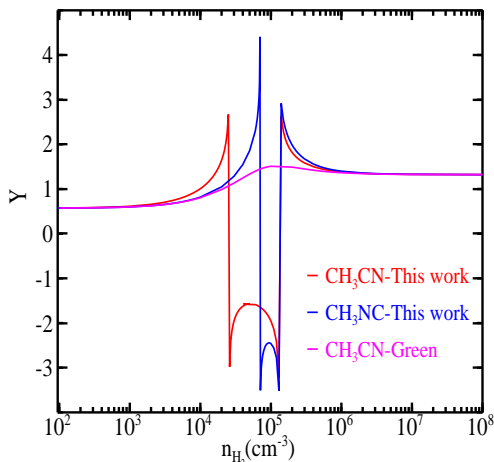


Figure 4. Variation of the logarithm of the excitation temperature as a function of the H_2 density for the $j_k = 2_1 \rightarrow 1_1$ CH_3CN and CH_3NC rotational transitions at kinetic temperature of 20 K. In order to better describe the large amplitude of its variation, the excitation temperature is represented on this figure as $Y = \frac{T_{ex}}{|T_{ex}|} \times \log_{10}(1 + |T_{ex}|)$. The results from the present work are compared to those obtained with the rate coefficients of Green (1986).

using recent accurate ab initio PESs. These cross sections were then averaged over a Maxwell-Boltzmann distribution of velocities to determine quenching collision rate coefficients between the first 74 levels of *para*- CH_3CN/NC and first 66 levels of *ortho*- CH_3CN/NC for temperatures ranging from 5 to 100 K. The rate coefficients for the two isomers display different propensity rules. Transitions with $\Delta j = 2, \Delta k = 0$ are dominant for CH_3CN -He collisions, while for CH_3NC -He a propensity rule is found in favour of $\Delta j = 1, \Delta k = 0$ transitions at low temperatures but $\Delta j = 2, \Delta k = 0$ at high temperatures. Overall the CH_3CN -He collision rate coefficients are found to be slightly smaller than those for CH_3NC -He isomer, which can be explained based on the depth of the potential energy surface corresponding to the collision, which is larger for CH_3NC -He than for CH_3CN -He (See paper I).

We have compared the new set of rate coefficients of CH_3CN -He with those available in literature for CH_3CN - H_2 that are currently used for astrophysical modeling. An important discrepancy was found between both sets of data, with differences of up to 3 orders of magnitude for some transitions. There does not seem to be any correlation between the two data sets, which demonstrates the usefulness of the present collisional rates. Even though the present calculations have been performed for the excitation with He atoms and not H_2 molecules, we recommend the use of these new rates in non-LTE models of CH_3CN excitation.

A systematic comparison of the excitation rate coefficients for CH_3CN -He and CH_3NC -He shows that the rates differ by up to a factor of 3. These isomerism effects in the collisional excitation show that separate calculations must be performed for each isomer as the rate coefficients cannot be assumed to be equal. These differences also let us predict that the excitation of these molecules in cold molecular clouds will be different, and we must use the appropriate rate coefficients of each isomer. To confirm this, we carried out a radiative transfer simulation for both isomers using scaled rate coefficients of CH_3CN/NC . As predicted, the comparison of both brightness and excitation temperatures demonstrates that the excitation is different

from one isomer to another and confirm again the need for separate analysis for both isomers.

In this paper, the collisional excitation of CH_3CN and CH_3NC with He atoms was carried out. He is often considered as a proxy for the spherical *para*- H_2 ($j=0$), especially for large molecules (more than 6 atoms) due to the larger complexity of the interaction and dynamics with H_2 (and the required computational resources needed to perform the calculations). Although this approximation is useful, it is often found that H_2 behaves differently than He in excitation studies, in particular for collisions involving *ortho*- H_2 . This deserves its own studies and will be the subject of future work.

ACKNOWLEDGEMENTS

J.L. acknowledges support from KU Leuven through Grant No. 19-00313.

REFERENCES

- Agúndez M., Fonfría J. P., Cernicharo J., Pardo J. R., Guélin M., 2008, *Astronomy & Astrophysics*, 479, 493
- Alexander M. H., Dagdigan P. J., Werner H.-J., Klos J., Desrousseaux B., Raffy G., Lique F., 2023, *Computer Physics Communications*, XXX, xxx
- Araya E., Hofner P., Kurtz S., Bronfman L., DeDeo S., 2005, *The Astrophysical Journal Supplement Series*, 157, 279
- Arthurs A. M., Dalgarno A., 1960, *Proceedings of the Royal Society of London. Series A. Mathematical and Physical Sciences*, 256, 540
- Bellili A., Gouid Z., Gazeau M., Bénilan Y., Fray N., Guillemin J., Hochlaf M., Schwell M., 2019, *Physical Chemistry Chemical Physics*, 21, 26017
- Belloche A., Garrod R., Müller H., Menten K., Comito C., Schilke P., 2009, *Astronomy & Astrophysics*, 499, 215
- Beltran M. T., Cesaroni R., Neri R., Codella C., Furuya R. S., Testi L., Olmi L., 2005, *Astronomy & Astrophysics*, 435, 901
- Ben Khalifa M., Dagdigan P. J., Loreau J., 2022, *J Phys Chem A*, 126
- Blackman G., Brown R., Godfrey P., Bassez M., Ottrey A., Winkler D., Robinson B., 1977, *Monthly Notices of the Royal Astronomical Society*, 180, 1P
- Bop C. T., Batista-Romero F. A., Faure A., Quintas-Sánchez E., Dawes R., Lique F., 2019, *ACS Earth and Space Chemistry*, 3, 1151
- Calcutt H., et al., 2018, *Astronomy & Astrophysics*, 617, A95
- Cazaux S., Tielens A., Ceccarelli C., Castets A., Wakelam V., Caux E., Parise B., Teyssier D., 2003, *The Astrophysical Journal*, 593, L51
- Cernicharo J., Kahane C., Guélin M., Gomez-Gonzalez J., 1988, *Astronomy and Astrophysics*, 189, L1
- Costain C., 1958, *The Journal of Chemical Physics*, 29, 864
- DeFrees D., McLean A., Herbst E., 1985, *The Astrophysical Journal*, 293, 236
- Dumouchel F., Faure A., Lique F., 2010, *Monthly Notices of the Royal Astronomical Society*, 406, 2488
- Dunning Jr T. H., 1989, *The Journal of chemical physics*, 90, 1007
- Endres C. P., Schlemmer S., Schilke P., Stutzki J., Müller H. S., 2016, *Journal of Molecular Spectroscopy*, 327, 95
- Gratier P., Pety J., Guzmán V., Gerin M., Goicoechea J., Roueff E., Faure A., 2013, *Astronomy & Astrophysics*, 557, A101
- Green S., 1976, *The Journal of Chemical Physics*, 64, 3463
- Green S., 1986, *The Astrophysical Journal*, 309, 331
- Hernández Vera M., Lique F., Dumouchel F., Klos J., Rubayo Soneira J., Senent M.-L., 2013, *Monthly Notices of the Royal Astronomical Society*, 432, 468
- Hutson J. M., Le Sueur R., 2019, *Computer Physics Communications*, 241, 9
- Irvine W. M., Schloerb F., 1984, *The Astrophysical Journal*, 282, 516
- Kawaguchi K., Ohishi M., Ishikawa S.-I., Kaifu N., 1992, *The Astrophysical Journal*, 386, L51
- Knizia G., Adler T. B., Werner H.-J., 2009, *The Journal of chemical physics*, 130, 054104

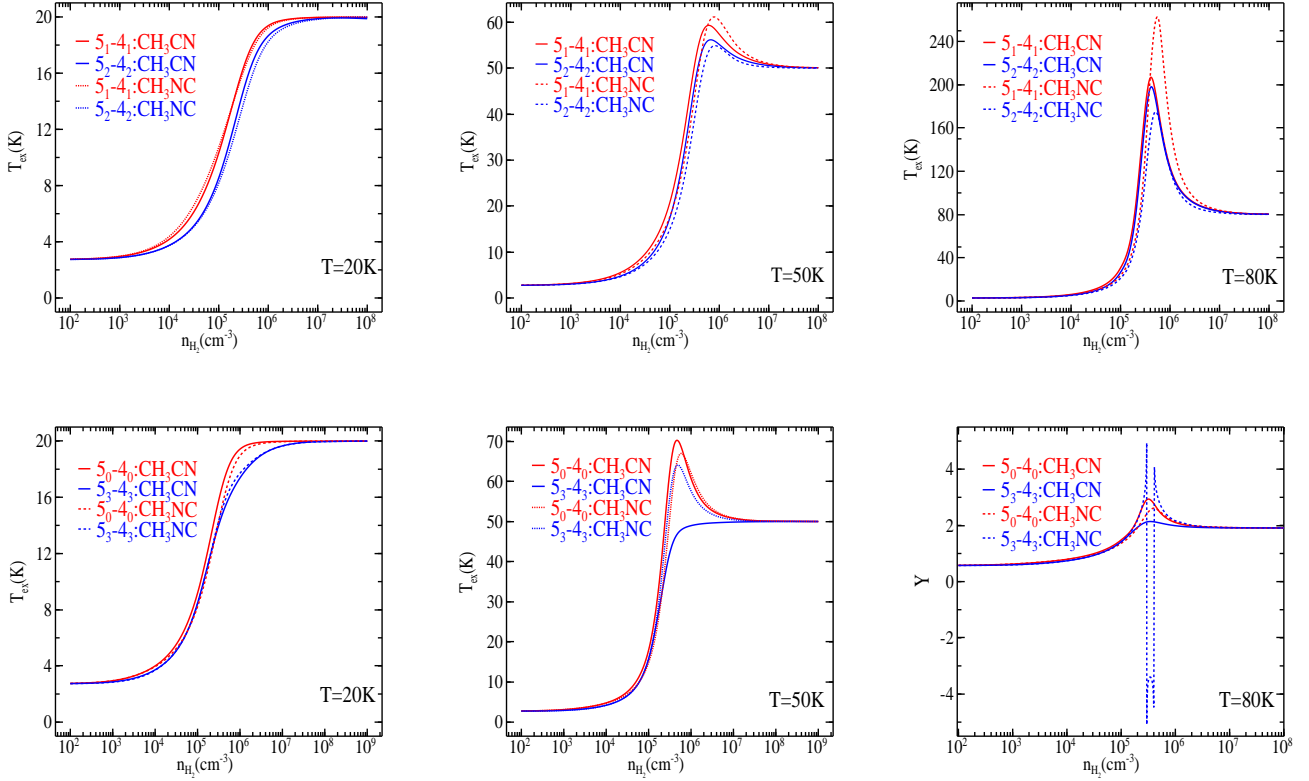


Figure 5. Excitation temperature of CH₃CN (solid curves) and CH₃NC (dashed curves) for the transitions $j_k \rightarrow j'_k$, with $j = 5$, $j' = 4$ and $k = k' = 1$ or 2 (*para*-CH₃CN/NC, top panels) and $k = k' = 0$ or 3 (*ortho*-CH₃CN/NC, bottom panels) as a function of the H₂ density for three kinetic temperature (20 K, 50 K and 80 K) and a column density of 10^{14} cm⁻². The bottom right panel shows $Y = \frac{T_{ex}}{|T_{ex}|} \times \log_{10}(1 + |T_{ex}|)$ instead of the excitation temperature.

- Lee P., Cohn K., Schwendeman R., 1972, *Inorganic Chemistry*, 11, 1920
López A., et al., 2014, *Astronomy & Astrophysics*, 572, A44
Loreau J., van der Avoird A., 2015, *J. Chem. Phys.*, 143, 184303
Loreau J., Liévin J., Scribano Y., van der Avoird A., 2014, *J. Chem. Phys.*, 141, 224303
Mackay D., 1999, *Monthly Notices of the Royal Astronomical Society*, 304, 61
Margulès L., Demaison J., Rudolph H., 2001, *Journal of molecular structure*, 599, 23
Margulès L., Tercero B., Guillemin J., Motiyenko R., Cernicharo J., 2018, *Astronomy & Astrophysics*, 610, A44
Matthews H. E., Sears T. J., 1983, *The Astrophysical Journal*, 267, L53
McElroy D., Walsh C., Markwick A., Cordiner M., Smith K., Millar T., 2013, *Astronomy & Astrophysics*, 550, A36
McGuire B. A., 2022, *The Astrophysical Journal Supplement Series*, 259, 30
McGuire P., Kouri D. J., 1974, *The Journal of Chemical Physics*, 60, 2488
McGuire B. A., Burkhardt A. M., Kalenskii S., Shingledecker C. N., Remijan A. J., Herbst E., McCarthy M. C., 2018, *Science*, 359, 202
Moffat J., 1964, *Canadian Journal of Chemistry*, 42, 1323
Müller H. S., Thorwirth S., Roth D., Winnewisser G., 2001, *Astronomy & Astrophysics*, 370, L49
Naouai M., Jrad A., Badri A., Najar F., 2021, *Monthly Notices of the Royal Astronomical Society*, 507, 5264
Nguyen T. L., Thorpe J. H., Bross D. H., Ruscic B., Stanton J. F., 2018, *The Journal of Physical Chemistry Letters*, 9, 2532
Öberg K. I., Guzmán V. V., Furuya K., Qi C., Aikawa Y., Andrews S. M., Loomis R., Wilner D. J., 2015, *Nature*, 520, 198
Pols S., Schwörer A., Schilke P., Schmiedeke A., Sánchez-Monge Á., Möller T., 2018, *Astronomy & Astrophysics*, 614, A123
Remijan A., Markwick-Kemper A., 2007, *BAAS*, 39, 963
Remijan A. J., Hollis J., Lovas F. J., Plusquellic D. F., Jewell P., 2005, *The Astrophysical Journal*, 632, 333
Roueff E., Lique F., 2013, *Chemical reviews*, 113, 8906
Schilke P., Benford D., Hunter T., Lis D., Phillips T., 2001, *The Astrophysical Journal Supplement Series*, 132, 281
Snyder L. E., Buhl D., 1972, *Annals of the New York Academy of Sciences*, 194, 17
Ulich B., Conklin E., 1974, *Nature*, 248, 121
Van der Tak F., Black J. H., Schöier F., Jansen D., van Dishoeck E. F., 2007, *Astronomy & Astrophysics*, 468, 627
Werner H.-J., et al., 2015, MOLPRO, version 2015.1, a package of ab initio programs
Willacy K., Williams D., Minh Y., 1993, *Monthly Notices Of The Royal Astronomical Society*, 263, L40
Wilner D., Wright M., Plambeck R., 1994, *The Astrophysical Journal*, 422, 642
Zapata L. A., Schmid-Burgk J., Muders D., Schilke P., Menten K., Guesten R., 2010, *Astronomy & Astrophysics*, 510, A2
Zeng S., Quénard D., Jiménez-Serra I., Martín-Pintado J., Rivilla V., Testi L., Martín-Doménech R., 2019, *Monthly Notices of the Royal Astronomical Society: Letters*, 484, L43

This paper has been typeset from a $\text{\TeX}/\text{\LaTeX}$ file prepared by the author.

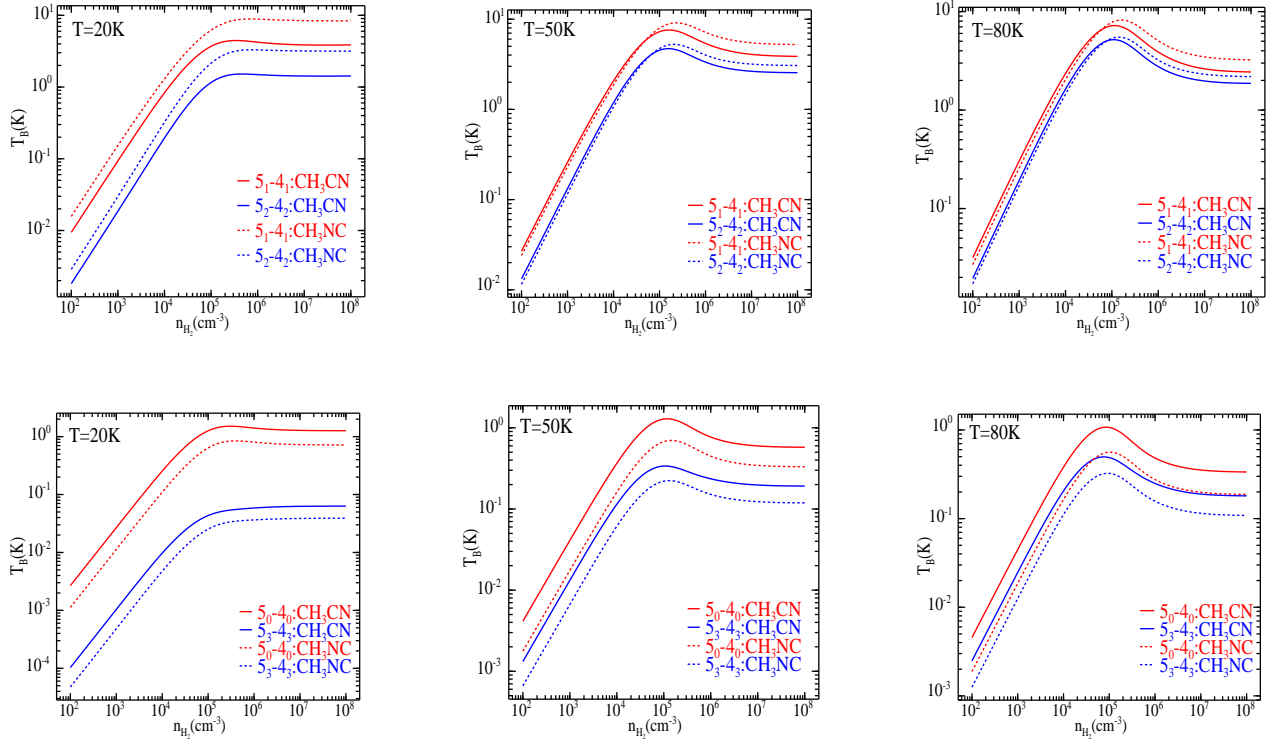


Figure 6. Brightness temperature of CH_3CN (solid curves) and CH_3NC (dashed curves) for the transitions $j_k \rightarrow j'_k$, with $j = 5$, $j' = 4$ and $k = k' = 1$ or 2 (*para*- $\text{CH}_3\text{CN/NC}$, top panels) and $k = k' = 0$ or 3 (*ortho*- $\text{CH}_3\text{CN/NC}$, bottom panels) as a function of the H_2 density for three kinetic temperature (20K, 50K and 80K) and a column density of 10^{14} cm^{-2} .